Vehicle Detection and Localization Using Unattended Ground Magnetometer Sensors

Carol T. Christou and Garry M. Jacyna
The MITRE Corporation
McLean, VA
Email: christou@mitre.org, gjacyna@mitre.org

***Abstract*—This analysis was completed as part of a larger Modeling and Simulation effort to estimate algorithm-level Measures of Performance (MOP), such as the probability of detection (PD) and the probability of identification (PID) of a vehicle or person transiting through an area of interest. The present work focuses on MOPs for Unattended Ground Magnetometer Sensors, which may be used to detect passing vehicles and estimate their bearing relative to the magnetometer position. In the first phase of the analysis, we concentrate on the probability of detection as a function of vehicle speed and distance (i.e., point of closest approach (CPA)) from the sensor. In the second phase, we try to localize the vehicle by extracting its relative bearing with respect to the magnetometer from the two orthogonal induced magnetic field measurements. The derivations are based on the assumption that a road vehicle may be approximated as a prolate homogeneous ellipsoid, as well as the assumption of uniform linear motion. Results show that, for speeds below 30 MPH, the maximum detection ranges (for PD = 0.5) are on the order of 40 meters for two-axis fluxgate magnetometers and for the operational parameters used in this analysis.**[1]

I. Introduction

The work described in this report focuses on the performance of magnetic Unattended Ground Sensors (UGS) in monitoring and reporting vehicle traffic on roads in an area of interest. The sensors are fluxgate magnetometers with built-in GPS, network based two-way communications and local communications to cue other sensors. The operating principles of fluxgate magnetometers are well documented, e.g., [1], [2]. Typical devices contain a primary ("drive") coil surrounded by a secondary ("sense") coil, with the primary coil wrapped around a permeable core material divided into two matched halves. When an alternating current is applied to the drive coil, the core material oscillates between positive and negative saturation. The instantaneous current in each core half is driven in opposite polarity to any external magnetic field. With no external field, the flux in one core half cancels that in the other and the total flux sensed by the secondary coil is zero. If an external field is applied, a net flux imbalance between the two core halves means that they no longer cancel each other. Current is now induced in the secondary coil on every primary current phase reversal, or at the second and higher even harmonics. This produces a signal that is a function of both the external field magnitude and polarity, [2]. Figure 1 is a schematic diagram of a fluxgate magnetometer with its external circuit. Thus, the device is capable of measuring the strength of any component of the Earth's magnetic field by simply rotating it so that the cores are parallel to the appropriate component. Fluxgate magnetometers are capable of measuring the strength of the magnetic field to about 0.5 to 1.0 nT. The instruments assumed in this analysis are two-axis magnetometers that can measure two perpendicular magnetic components of the external field simultaneously. Other factors also influence the strength of the output signal. These include the number of turns in the windings, the core magnetic permeability, the sensor geometry and the gated flux rate of change with time. Phase synchronous detection is used to convert the harmonic signals to a DC voltage proportional to the external magnetic field [3]. High quality low noise fluxgates use a feedback loop to keep the core at zero field. A phase synchronous detector (or analog multiplier) is used to detect the even harmonics and these signals are integrated in an analog integrator to develop a voltage that reflects the ambient field through the core. This signal is then fed back to the core to null it to zero, [2].

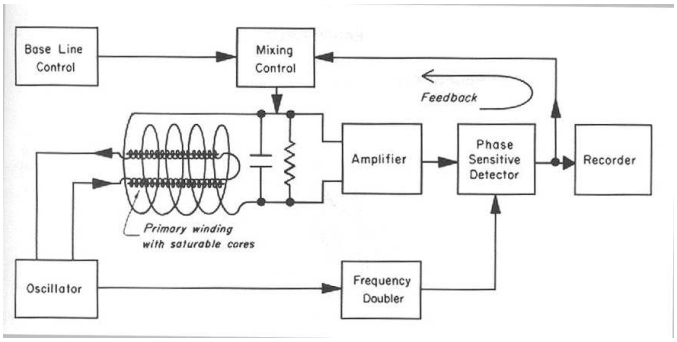

Figure 1. Operation of a Fluxgate Magnetometer.

Such magnetometers may be used for surveillance purposes by being placed close to roads ($\lesssim$ 40 m) carrying vehicular traffic. Because motorized ground vehicles (e.g., trucks, SUVs, cars) are traditionally comprised of nontrivial quantities of magnetic materials, they will exhibit a magnetic moment induced by the earth's magnetic field. In addition, the vehicle may also have an associated permanent moment, which depends on its magnetic history and manufacturing process. This may be an issue primarily for heavy armored vehicles. The commercial type vehicles that this work focuses on do

[1]Approved for Public Release: 10-0535. Distribution Unlimited.

not exhibit permanent magnetic moments due to modern manufacturing processes. This is because the forging temperature is well above the Curie temperature, and as the vehicle cools down its magnetic material does not align with the earth's magnetic field. At ranges much greater than its size, the target behaves like a magnetic dipole and can be detected and tracked as such. Because the induced moment is much smaller than the magnitude of the earth's magnetic field, the latter will have to be filtered out of the received signal with a high-pass filter, in order to allow detection of the weaker signal. As opposed to previous work, e.g., [4], this analysis assumes two-axis magnetometers. We also present an innovative detector scheme based on a matched filter and perform explicit calculations of the terrestrial magnetic field components in the body axes frame of the vehicle.

Section II contains a derivation of the magnetization of a metallic vehicle by the earth's magnetic field and the magnetic signal components received by the magnetometer. Section III focuses on the processing steps in the generation of a matched filter, which the detection is based on. Section IV discusses the inversion of the received magnetic field signals to back out a bearing relative to the sensor. Implementation details and results are presented in Section V, while Section VI contains the conclusions and discussion of future work.

II. Induced Magnetization

In order to get a closed form solution for the vehicle magnetization (moment per unit volume), we approximate the vehicle shape as a prolate homogeneous ellipsoid of revolution with axes $A \geq B \geq C$ and B = C. This has previously been shown to be a reasonable approximation for light, as well as heavy vehicles, [4]. Based on detailed calculations by Osborn, [5], the demagnetization factors L_1, L_2 in the longitudinal and transverse directions of the body in International System (SI) units are:

$$\begin{aligned} m &\equiv \frac{A}{B}, \quad c \equiv \sqrt{m^2-1}); \\ t_1 &= \frac{m}{2c}\log\left(\frac{m+c}{m-c}\right) - 1; \quad t_2 = m - t_1 - 1; \\ L_1 &= \frac{t_1}{c^2}; \quad L_2 = 0.5m\frac{t_2}{c^2}. \end{aligned} \tag{1}$$

We next construct the magnetic polarizability tensor:

$$P = \begin{pmatrix} \frac{\kappa}{(1+\kappa L_1)} & 0 & 0 \\ 0 & \frac{\kappa}{(1+\kappa L_2)} & 0 \\ 0 & 0 & \frac{\kappa}{(1+\kappa L_2)} \end{pmatrix}, \tag{2}$$

where κ represents the material magnetic susceptibility. The induced moment of the object is then:

$$M = VPH, \quad \text{where} \quad V = 4\pi\frac{AB^2}{3} \tag{3}$$

is the volume of the ellipsoid. H is the earth's magnetic field strength rotated to the body axes frame of the vehicle:

$$\begin{aligned} H &= H_0 \begin{pmatrix} \sin(\theta_C) & \cos(\theta_C) & 0 \\ -\cos(\theta_C) & \sin(\theta_C) & 0 \\ 0 & 0 & 1 \end{pmatrix} \\ &\quad \times \begin{bmatrix} \sin(\phi_d)\cos(\phi_i) \\ \cos(\phi_d)\cos(\phi_i) \\ \sin(\phi_i) \end{bmatrix}, \\ H_0 &= \frac{2.5B_0}{\pi}, \end{aligned} \tag{4}$$

where B_0 is the terrestrial magnetic induction in μTesla, ϕ_i is the magnetic inclination angle at that particular location, ϕ_d the magnetic declination angle and θ_C is the vehicle course with respect to true North.

Finally, the longitudinal and transverse magnetic field components for a dipole are [6]:

$$\begin{aligned} B_1 &= 10^{-7}\frac{M(1)(3x^2-R^2)+3M(2)xy}{R^5}; \\ B_2 &= 10^{-7}\frac{M(2)(3y^2-R^2)+3M(1)xy}{R^5}; \end{aligned} \tag{5}$$

where R is the range from the sensor to the vehicle, and x, y are the components of the range. It must be noted that this is only an approximation of a general source's field and is valid for R greater than the typical source dimensions (farfield approximation). B_1 and B_2 are now expressed in Tesla.

III. Matched Filter and Detector

First, we calculate the geomagnetic noise spectrum, as derived in [7]:

$$S_n(f_\ell) = \frac{(10^{-12}N_h)^2}{f_\ell}, \tag{6}$$

where N_h is the noise spectral level in pTesla/sqrt(Hz) (referenced to f_0 = 1 Hz), and f_ℓ, $\ell = 1, ..., N$ is the frequency which is determined by the magnetometer sampling rate, F_s, and observation time, $T_{obs} = N/F_s$. F_s in turn is given by $2B$, where B is the bandwidth of the magnetometer. Noise spectral levels can range from near 1 pTesla/sqrt(Hz) in rural land areas, to $>$ 100 pTesla/sqrt(Hz) in urban areas and roughly 10 pTesla/sqrt(Hz) near water. The sensor sensitivity noise spectrum may be derived by treating the magnetometer sensitivity as quantization noise. The sensitivity is basically the resolution of the device, Δ. If we assume that the signal is uniformly distributed within a resolution cell, the variance becomes:

$$\sigma^2 \equiv E(s^2) = \frac{1}{\Delta}\int_{-\frac{\Delta}{2}}^{\frac{\Delta}{2}} x^2 dx = \frac{\Delta^2}{12}. \tag{7}$$

The spectral density is then flat and is of the form:

$$S_s(f_\ell) = \frac{\Delta^2}{24B}; \quad -B \leq f_\ell \leq B, \tag{8}$$

where B is the bandwidth of the device (typically 5 - 10 Hz). We next obtain the combined noise spectrum by adding the

sensor sensitivity spectrum to the background noise spectrum, $S_{noise} = S_n + S_s$.

A high-pass filter is required in order to remove the large terrestrial magnetic field component near DC. In our work this is implemented as a simple boxcar filter $H_{hp} = 0$ if the frequency f is lower than a cut-off frequency F_{cut}, which here was set equal to 2 Hz. Otherwise, $H_{hp} = 1$. After obtaining the Fourier Tranforms $\widetilde{B}_1$, $\widetilde{B}_2$ of signals B_1 and B_2 from Eq. (5), the matched filter is computed as:

$$\begin{aligned} d_1^2 &= \frac{F_s}{N}\sum_{\ell=1}^{N}\frac{|\widetilde{B}_1(f_\ell)|^2}{S_{noise}(f_\ell)}, \\ d_2^2 &= \frac{F_s}{N}\sum_{\ell=1}^{N}\frac{|\widetilde{B}_2(f_\ell)|^2}{S_{noise}(f_\ell)}. \end{aligned} \tag{9}$$

It is noted that the proper normalizations must be included for $\widetilde{B}_1$, $\widetilde{B}_2$, d_1 and d_2 to approximate true integrations. Detailed derivations may be found in the Appendix. The deflection ratio is then:

$$d = (d_1^2 + d_2^2)^{\frac{1}{2}}. \tag{10}$$

Assuming that $\widetilde{B}_1$, $\widetilde{B}_2$ are Gaussian distributed, the probability of detection, PD, is:

$$\begin{aligned} PD &= Prob(\gamma > \eta | H_1) \\ &= \left(\frac{1}{2\pi\sigma_i^2}\right)^{\frac{1}{2}}\int_{\eta}^{\infty}\exp\left[-\frac{(s-m_i)^2}{2\sigma_i^2}\right]ds \\ &= \left(\frac{1}{2\pi}\right)^{\frac{1}{2}}\int_{\frac{\eta-m_i}{\sigma_i}}^{\infty}\exp\left[-\frac{s^2}{2}\right]ds = \Phi\left(\frac{\eta-m_i}{\sigma_i}\right), \end{aligned} \tag{11}$$

where Φ is the modified complimentary error function, γ is the sufficient statistic derived in the Appendix and η is a threshold. The probability of false alarm is then $PFA = Prob(\gamma > \eta|H_0) = \Phi\left(\frac{\eta}{\sigma_i}\right)$. Let $\eta' \equiv \frac{\eta}{\sigma_i}$. Then

$$PFA = \Phi(\eta'), \tag{12}$$

$$PD = \Phi(\eta' - d_i). \tag{13}$$

If we fix the value of PFA, then we must invert the error function $\Phi(\eta\prime)$ to find the corresponding threshold η'. We then substitute this value into Eq. (13) to find PD.

IV. Localization through Bearing Estimation

Figure 2 shows an example scenario for detection of a truck by a magnetometer placed near a roadway. In this case, the truck course is 90^o from true North. We begin with Eq. (5) for the signals B_1 and B_2 received by the magnetometer from the longitudinal and transverse magnetic moments of the vehicle. We further assume that the large earth magnetic field components have been filtered out. If we divide the first by the second equation and cross-multiply, we get:

$$B_1 m_2(2y^2 - x^2) + 3B_1 m_1 xy = B_2 m_1(2x^2 - y^2) + 3B_2 m_2 xy, \tag{14}$$

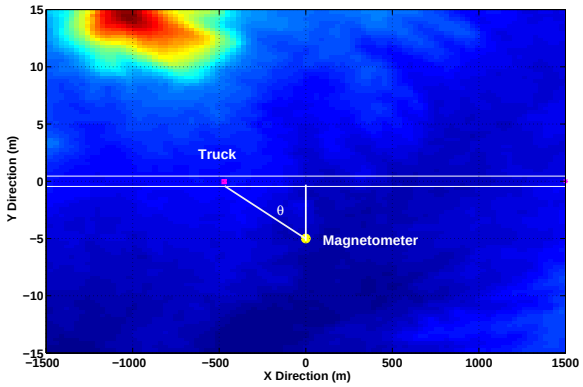

Figure 2. Example Scenario for a Magnetometer Near a Road.

where $m_1 = M(1)$ and $m_2 = M(2)$ denote the longitudinal and transverse magnetic moments of the vehicle, respectively. If the coordinate system is oriented so that x lies along the straight road direction and y lies perpendicular, then y is constant and equal to CPA. If we also assume reasonable prior estimates of m_1 and m_2, Eq. (14) may be solved for x at each time $t = n/F_s$ in the observation period, where F_s is the sampling frequency, $n = [0 : N]$ and $N = F_s T_{obs}$. In the present analysis, F_s = 22 sec^{-1}, T_{obs} = 0.5 sec, and N = 11. This results in a quadratic equation with two solutions, only one of which is physically acceptable:

$$\begin{aligned} x &= \frac{-B + \sqrt{B^2 - 4AC}}{2A}, \\ A &= 2B_2 m_1 + B_1 m_2; \quad B = 3(B_2 m_2 y - B_1 m_1 y); \\ C &= -y^2(B_2 m_1 + 2B_1 m_2). \end{aligned} \tag{15}$$

The relative bearing from the magnetometer to the vehicle is $\theta = \arctan(y/x)$. The results are then averaged over all times t to get a mean bearing estimate in a particular observation period. If the magnetic moments are unknown, it is necessary to have measurements from more than one magnetometer in order to solve for three unknowns. Figure 3 shows an example scenario with three magnetometers placed at different locations on either side of the road. First, let us consider the magnetometers 1 and 2, whose coordinates with respect to the vehicle are $(x_1,\ y_1)$, $(x_2,\ y_2)$. Denoting the ratios of B_1 to B_2 as $\alpha_1,\ \alpha_2$ for the two magnetometers, we have from Eq. (5)

$$\begin{aligned} \alpha_1(m_2(2y_1^2 - x_1^2) + 3m_1 x_1 y_1) &= m_1(2x_1^2 - y_1^2) \\ &+ 3m_2 x_1 y_1; \\ \alpha_2(m_2(2y_2^2 - x_2^2) + 3m_1 x_2 y_2) &= m_1(2x_2^2 - y_2^2) \\ &+ 3m_2 x_2 y_2. \end{aligned} \tag{16}$$

Rearranging Eqs. (16) and then dividing the first by the second,

we get:

$$\begin{aligned}&(\alpha_1(2y_1^2 - x_1^2) - 3x_1y_1)(2x_2^2 - y_2^2 - 3\alpha_2 x_2 y_2)\\ -\ &(2x_1^2 - y_1^2 - 3\alpha_1 x_1 y_1)(\alpha_2(2y_2^2 - x_2^2) - 3x_2y_2) = 0,\end{aligned} \tag{17}$$

where $y_1,\ y_2$ are the known perpendicular distances of the sensors from the road. Substituting $x_2 = x_1 - x_0$, where x_0 is the known x distance between the sensors, we obtain a quartic equation in x_1:

$$\begin{aligned}&Ax_1^4 + Bx_1^3 + Cx_1^2 + Dx_1 + E = 0,\\ A &= 2\alpha_2 - 2\alpha_1,\\ B &= 4\alpha_1 x_0 - 4\alpha_2 x_0 - 6y_1 - 3\alpha_1\alpha_2 y_1 + 6y_2 + 3\alpha_1\alpha_2 y_2,\\ C &= -2\alpha_1 x_0^2 + 2\alpha_2 x_0^2 + 12x_0y_1 + 6\alpha_1\alpha_2 x_0 y_1 + 4\alpha_1 y_1^2\\ &- \alpha_2 y_1^2 - 6x_0y_2 - 3\alpha_1\alpha_2 x_0 y_2 - 9\alpha_1 y_1 y_2 + 9\alpha_2 y_1 y_2\\ &+ \alpha_1 y_2^2 - 4\alpha_2 y_2^2,\\ D &= -6x_0^2 y_1 - 3\alpha_1\alpha_2 x_0^2 y_1 - 8\alpha_1 x_0 y_1^2 + 2\alpha_2 x_0 y_1^2\\ &+ 9\alpha_1 x_0 y_1 y_2 - 9\alpha_2 x_0 y_1 y_2 - 3y_1^2 y_2 - 6\alpha_1\alpha_2 y_1^2 y_2\\ &+ 3y_1 y_2^2 + 6\alpha_1\alpha_2 y_1 y_2^2,\\ E &= 4\alpha_1 x_0^2 y_1^2 - \alpha_2 x_0^2 y_1^2 + 3x_0 y_1^2 y_2 + 6\alpha_1\alpha_2 x_0 y_1^2 y_2\\ &- 2\alpha_1 y_1^2 y_2^2 + 2\alpha_2 y_1^2 y_2^2.\end{aligned} \tag{18}$$

Dividing the first of Eqs. (18) by A, the quartic equation becomes normalized such that now the coefficient of x_1^4 is one and the other new coefficients are $C''_{3,2,1,0} = (B,\ C,\ D,\ E)/A$. The next step is to find the real root z_1 of the resolvent cubic equation:

$$\begin{aligned}x_1^3 &- C''_2 x_1^2 + (C''_1 C''_3 - 4C''_0)x_1 + (4C''_2 C''_0 - C_1^{''2}\\ &- C_3^{''2} C''_0) = x_1^3 + C'_2 x_1^2 + C'_1 x_1 + C'_0 = 0.\end{aligned} \tag{19}$$

Finally, the four roots of the quartic Eq. (18) are

$$\begin{aligned}x_1(1) &= -\frac{C''_3}{4} + \frac{RR}{2} + \frac{D'}{2};\\ x_1(2) &= -\frac{C''_3}{4} + \frac{RR}{2} - \frac{D'}{2};\\ x_1(3) &= -\frac{C''_3}{4} - \frac{RR}{2} + \frac{E}{2};\\ x_1(4) &= -\frac{C''_3}{4} - \frac{RR}{2} - \frac{E}{2},\end{aligned} \tag{20}$$

where

$$RR = \sqrt{\frac{C_3^{''2}}{4} - C''_2 + z_1};$$

$$\text{if}\quad RR = 0: \quad D' = \sqrt{\frac{3C_3^{''2}}{4} - 2C''_2 + 2\sqrt{z_1^2 - 4C''_0}};$$

$$E = \sqrt{\frac{3C_3^{''2}}{4} - 2C''_2 - 2\sqrt{z_1^2 - 4C''_0}};$$

$$\text{else}:$$

$$D' = \sqrt{\frac{3C_3^{''2}}{4} - RR^2 - 2C''_2 + \frac{4C''_3 C''_2 - 8C''_1 - C_3^{''3}}{4RR}};$$

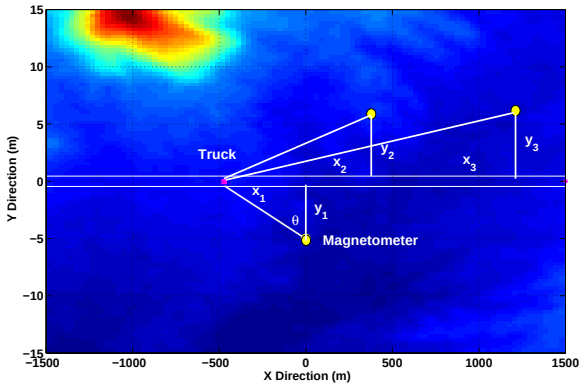

Figure 3. Example Scenario for Three Magnetometers Near a Road.

$$E = \sqrt{\frac{3C_3^{''2}}{4} - RR^2 - 2C''_2 - \frac{4C''_3 C''_2 - 8C''_1 - C_3^{''3}}{4RR}}, \tag{21}$$

and

$$\begin{aligned}z_1 &= -\frac{C'_2}{3} + S + T;\\ S &= \sqrt[3]{G + \sqrt{D}};\ \ T = \sqrt[3]{G - \sqrt{D}};\\ Q &= \frac{3C'_1 - C_2^{'2}}{9};\ \ G = \frac{9C'_2 C'_1 - 27C'_0 - 2C_2^{'3}}{54};\\ D &= Q^3 + G^2.\end{aligned} \tag{22}$$

Care must be taken in choosing the physically correct solution out of the four. First, any complex solutions must be discarded, and the remainder checked for consistency with the assumptions. The bearings from the magnetometers to the vehicle are then $\theta_1 = \arctan(y_1/x_1)$ and $\theta_2 = \arctan(y_2/x_2)$. Substituting the solution for x_1 in the first of Eqs. (16), we may solve for the ratio $m' \equiv m_2/m_1$:

$$m' = \frac{(2x_1^2 - y_1^2 - 3\alpha_1 x_1 y_1)}{(\alpha_1(2y_1^2 - x_1^2) - 3x_1 y_1)}. \tag{23}$$

In order to obtain solutions for m_1, m_2 separately, we need measurements from three sensors, as shown in Figure 3.

V. Implementation and Results

Initially, calculations were performed for one observation time interval (T_{obs} = 0.5 sec) around CPA. The PD was calculated as a function of CPA and speed for a heavy vehicle (length = 7.1 m, width = 3.25 m) and a light vehicle (length = 4 m, width = 2 m). Table I contains the parameters used in the simulations:

Figure 2, as stated previously, shows an example scenario for detection of a truck by a magnetometer placed near a roadway. In this case, the truck course is 90^o from true North. Figure 4 contains image plots of the PD as a function of CPA of the vehicle to the magnetometer in meters and vehicle speed, V, in MPH. Plot 4(a) corresponds to the truck and plot 4(b) to the car.

Magnetic inclination angle	40^o
Magnetic declination angle	-5^o
Magnetic field	70 μTesla
Material magnetic susceptibility	10
Noise spectral level	100 pTesla/sqrt(Hz)
Observation time	0.5 sec
High-pass filter cut-off	3 Hz
Magnetometer bandwidth	11 Hz
Magnetometer sensitivity	9×10^{-10} Tesla
PFA	1×10^{-6}

Table I
SIMULATION PARAMETERS.

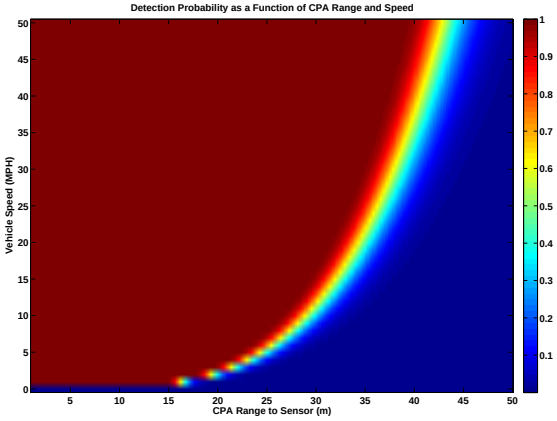

(a)

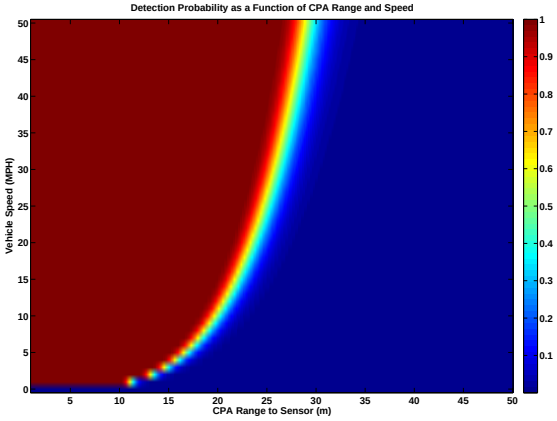

(b)

Figure 4. PD versus CPA and V for (a) Truck and (b) Car.

Figure 5 contains contour plots of three PD values, equal to 0.5, 0.9 and 0.95, as a function of CPA of the vehicle to the magnetometer in meters and vehicle speed, V, in MPH. Plot 5(a) corresponds to the truck and plot 5(b) to the car. We see from both of the above figures that for a fixed PD and speed, the CPA (here, y distance) for detection at that PD level is about 15 m longer for a heavy vehicle than for a light one. This could potentially help with classification.

In the next phase, PD values were found for successive observation time intervals corresponding to various x distances

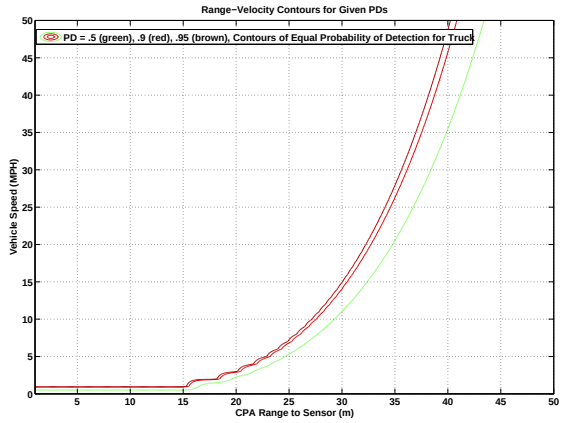

(a)

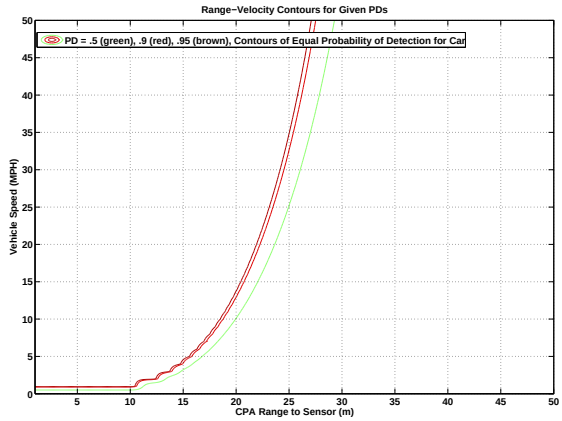

(b)

Figure 5. PD Contour Plots for (a) Truck and (b) Car.

(distance along direction of the straight road) from the magnetometer. While the x direction is in general taken to be along the road, the y direction is in a perpendicular direction from the magnetometer position to the road. In this manner, the calculated bearing is always with respect to the magnetometer. The initial points of motion were taken around x = − 60 m, while the final points were roughly symmetrical with respect to CPA, which was varied from 5 to 40 m in steps of 5 m. The calculations were repeated for a truck and a car at speeds of 20 and 40 MPH. Plots of PD versus x distance are shown in Figure 6. We see that, as the CPA increases, the x range of detectability narrows, slowly at first, and then in a discontinuous fashion after 30 m for a truck at 20 MPH, 35 m for a truck at 40 MPH, 20 m for a car at 20 MPH and 25 m for a car at 40 MPH. Comparing plots 6(a) with 6(c) and 6(b) with 6(d), we again notice that, for equal speeds, detectability horizontal ranges (x distances) for trucks exceed those for cars by about 15 m. We find that, for equal speeds again, detectability (slant) ranges for trucks are ∼20 m longer than for cars.

Results for bearing estimation for the same parameters of Table 1, assuming measurements from one sensor and a priori

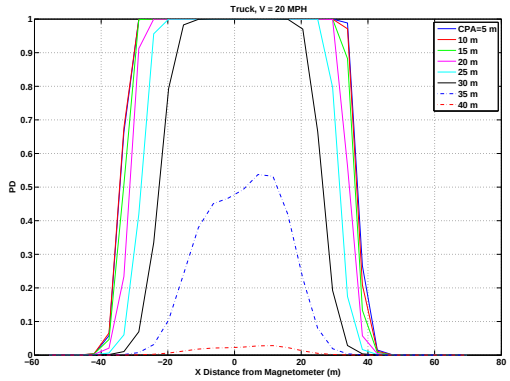

(a)

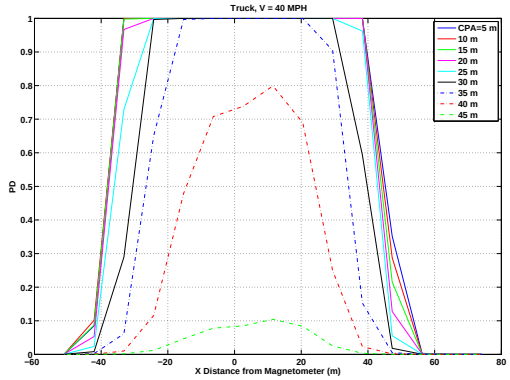

(b)

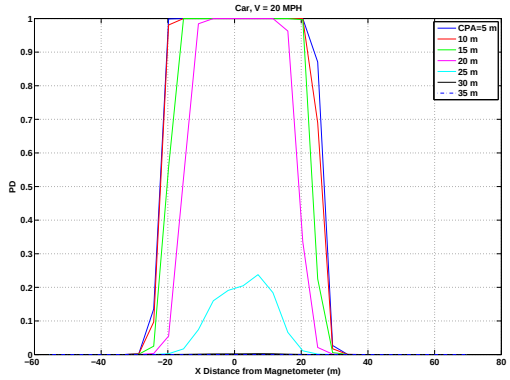

(c)

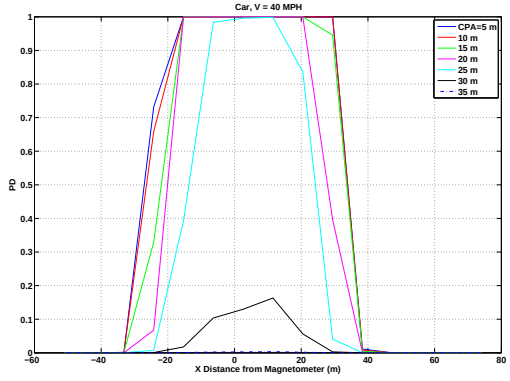

(d)

Figure 6. PD versus X Distance for (a) Truck at 20 MPH, (b) Truck at 40 MPH, (c) Car at 20 MPH, (d) Car at 40 MPH.

knowledge of the magnetization magnitudes, are presented in Figure 7. Comparing Figures 7(a) with 7(c) and 7(b) with 7(d), we see that, with prior knowledge of the magnetizations, the bearings are independent of the vehicle type for the same speed.

VI. Conclusions

The MITRE Corporation has undertaken a preliminary simulation of a surveillance scenario to estimate algorithm-level MOPs. This analysis is part of that effort and focuses on UGS two-axis fluxgate magnetometers which will be placed close to roadways in order to detect and localize vehicular traffic through the area. Assuming uniform linear motion, the detection probabilities of a moving vehicle are calculated as functions of speed and CPA from the sensor. The received signals are a function of distance (range R, x and y coordinates) from the magnetometer, as well as magnetization of the vehicle induced by the earth's magnetic field. This, in turn, depends on the vehicle dimensions and material. The received orthogonal signals are then processed through Fourier Transformation and derivation of a matched filter. Assuming a fixed PFA level, the PD is then found as a function of the total deflection. Analyses were performed for heavy versus light vehicles, with results that differed enough to be able to develop a classification scheme in the next phase. It was found that, for equal speeds, the detection ranges for a heavy vehicle exceeded those for a light vehicle by about 20 m. Localization may best be achieved by combining multiple sensor measurements in order to solve for the relative bearing, as well as the magnetic moments of the vehicle. Assuming no permanent magnetization, if one has prior knowledge of at least the magnetic moment ratios, one may solve for the bearing as a function of observation time interval from only a single magnetometer. Prior knowledge of magnetic moment ratios would be possible if only certain types of vehicles were known to travel along the route of interest. Any subsequent work in the simulation of information extraction from magnetometer measurements will involve more detailed fusion of data from multiple sensors, as well as classification of vehicles into rough categories (heavy, medium size and very light).

References

[1] *A Review of Magnetic Sensors*, J. E. Lenz, Proceedings of the IEEE, vol. 78, no. 6, pp. 973-989, June, 1990.

[2] *Fluxgate Magnetometers*, E. M. Billingsley and S. W. Billingsley, Proceedings of the SPIE, Volume 5090, pp. 194-203, 2003.

[3] *Tuned vs. Untuned Output*, P. Ripka and S.W. Billingsley, IEEE Trans. Magn. Volumme 34, pp. 1303-1305, 1998.

[4] *Magnetic localization and identification of vehicles*, L. Merlat and P. Naz, Proc. of SPIE, Volume 5090, pp. 174-185, 2003.

[5] *Demagnetizing Factors of the General Ellipsoid*, J. A. Osborn, Phys. Rev., vol. 67, nos 11 and 12, pp. 351-357, 1945.

[6] *Classical Electrodynamics*, J. D. Jackson, Third Edition, New York Academic Press, 1998, pp. 184-188.

[7] *What and Where is the Natural Noise Floor?*, J. Meloy, Third Edition, www.vlf.it/naturalnoisefloor/naturalnoisefloor.htm, 2003.

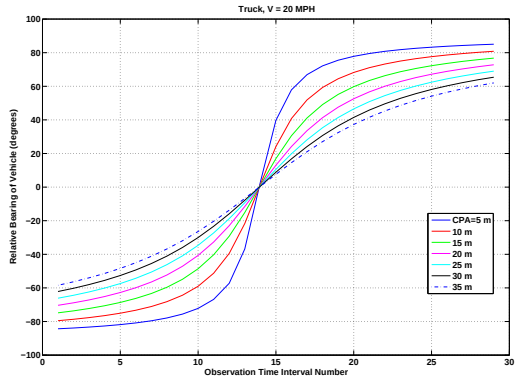

(a)

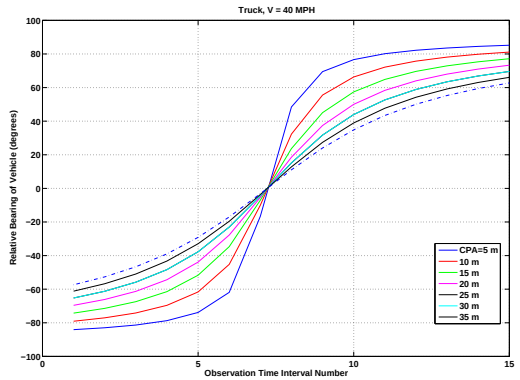

(b)

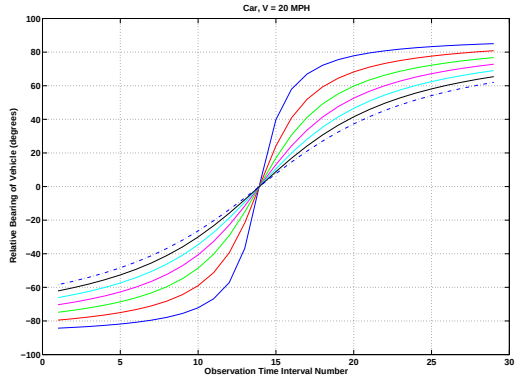

(c)

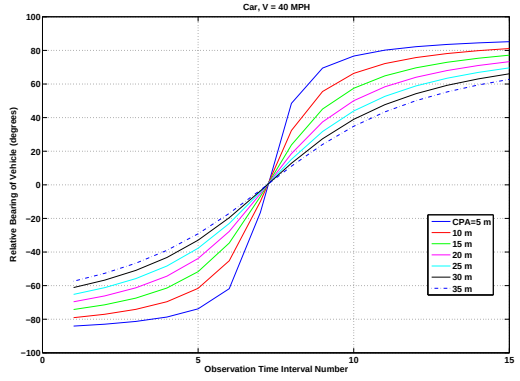

(d)

Figure 7. Extracted Bearings versus Observation Time Interval Number for (a) Truck at 20 MPH, (b) Truck at 40 MPH, (c) Car at 20 MPH, (d) Car at 40 MPH.

APPENDIX

Let $B_i(t) = B_i^o(t) + n_i(t),\ i = 1, 2$, where t is the time, $B_i^o(t)$ is the true induced magnetic field in the planar directions $(i = 1, 2)$ and $n_i(t)$ is zero-mean Gaussian $\frac{1}{f}$ noise assumed independent for $i = 1, 2$. Let the Fourier Transform (FT) of $B_i(t)$ be $\widetilde{B}_i(f_\ell)$, where $f_\ell = \frac{\ell-1}{N}F_s$, $\ell = 1, 2, ...N$, $F_s = \frac{1}{\Delta T}$, ΔT is the time increment and $T \equiv N\Delta T$ is the observation time. Assume two hypotheses, H_1 when a signal is present and H_0, when only noise is present. Noting that

$$E(|\widetilde{B}_i(f_\ell)|^2|H_0) = E(|\widetilde{N}_i(f_\ell)|^2) \equiv TS_n(f_\ell), \tag{24}$$

where $S_n(f_\ell)$ is the noise spectrum[2], we have for the probability of $\widetilde{B}_i$ under both hypotheses:

$$\begin{aligned} P(\widetilde{B}_i|H_1) &= C\exp\left[-\sum_{\ell=1}^{\frac{N}{2}}\frac{|\widetilde{B}_i(f_\ell) - \widetilde{B}_i^o(f_\ell)|^2}{TS_n(f_\ell)}\right], \\ P(\widetilde{B}_i|H_0) &= C\exp\left[-\sum_{\ell=1}^{\frac{N}{2}}\frac{|\widetilde{B}_i(f_\ell)|^2}{TS_n(f_\ell)}\right], \end{aligned} \tag{25}$$

where C is a constant and only the positive frequency components $(\ell = 1, 2, ..., \frac{N}{2})$ are examined. Therefore, the likelihood ratio is:

$$\Lambda(\widetilde{B}_i) = \exp\left[2Real\sum_{\ell=1}^{\frac{N}{2}}\frac{\widetilde{B}_i^{o*}(f_\ell)\widetilde{B}_i(f_\ell)}{TS_n(f_\ell)}\right]K, \tag{26}$$

where K is a constant independent of the data. The sufficient statistic is:

$$\begin{aligned} \gamma_i &= Real\left[\sum_{\ell=1}^{\frac{N}{2}}\frac{\widetilde{B}_i^{o*}(f_\ell)\widetilde{B}_i(f_\ell)}{S_n(f_\ell)}\right] \\ &= \sum_{\ell=1}^{\frac{N}{2}}\left(\left(\widetilde{B}_i^{or}(f_\ell)\widetilde{B}_i^r(f_\ell) + \widetilde{B}_i^{oi}(f_\ell)\widetilde{B}_i^i(f_\ell)\right)/S_n(f_\ell)\right), \\ \widetilde{B}_i(f) &\equiv \widetilde{B}_i^r(f) + j\widetilde{B}_i^i(f), \quad j = \sqrt{-1}. \end{aligned} \tag{27}$$

Now,

$$\begin{aligned} E(\widetilde{B}_i^r) &= E(\widetilde{B}_i^{oi}) = 0 \quad \text{under} \quad H_0, \\ E(\widetilde{B}_i^r) &= \widetilde{B}_i^{or},\ E(\widetilde{B}_i^i) = \widetilde{B}_i^{oi} \quad \text{under} \quad H_1, \\ \sigma^2(\widetilde{B}_i^r) &= E(\widetilde{B}_i^{r2}|H_0) = T\frac{S_n(f_\ell)}{2}, \\ \sigma^2(\widetilde{B}_i^i) &= E(\widetilde{B}_i^{i2}|H_0) = T\frac{S_n(f_\ell)}{2}, \\ E(\widetilde{B}_i^r\widetilde{B}_i^i|H_0) &= 0. \end{aligned} \tag{28}$$

[2]If incorporating the sensor sensitivity noise spectrum S_s, replace S_n by $S_{noise} = S_n + S_s$.

This implies:

$$\begin{aligned} E(\gamma_i|H_0) &= 0, \\ E(\gamma_i|H_1) &= \sum_{\ell=1}^{\frac{N}{2}} \frac{(\widetilde{B}_i^{or2} + \widetilde{B}_i^{oi2})}{S_n(f_\ell)} \\ &= \sum_{\ell=1}^{\frac{N}{2}} \frac{|\widetilde{B}_i^o(f_\ell)|^2}{S_n(f_\ell)} \equiv m_i, \\ \sigma^2(\gamma_i|H_0,H_1) &= \sum_{\ell=1}^{\frac{N}{2}} \frac{\left(\frac{TS_n(f_\ell)}{2}\widetilde{B}_i^{or2} + \frac{TS_n(f_\ell)}{2}\widetilde{B}_i^{oi2}\right)}{S_n^2(f_\ell)} \\ &= \frac{T}{2}\sum_{\ell=1}^{\frac{N}{2}} \frac{|\widetilde{B}_i^o(f_\ell)|^2}{S_n(f_\ell)} \equiv \sigma_i^2. \end{aligned} \tag{29}$$

So, the probability of detection, PD is:

$$\begin{aligned} PD &= Prob(\gamma > \eta|H_1) \\ &= \left(\frac{1}{2\pi\sigma_i^2}\right)^{\frac{1}{2}} \int_\eta^\infty \exp\left[-\frac{(s-m_i)^2}{2\sigma_i^2}\right] ds \\ &= \left(\frac{1}{2\pi}\right)^{\frac{1}{2}} \int_{\frac{\eta-m_i}{\sigma_i}}^\infty \exp\left[-\frac{s^2}{2}\right] ds = \Phi\left(\frac{\eta-m_i}{\sigma_i}\right), \end{aligned} \tag{30}$$

while the probability of false alarm $PFA = Prob(\gamma > \eta|H_0) = \Phi\left(\frac{\eta}{\sigma_i}\right)$. Let $\eta' \equiv \frac{\eta}{\sigma_i}$. Then $PFA = \Phi(\eta')$, $PD = \Phi(\eta' - d_i)$, where

$$d_i \equiv \frac{m_i}{\sigma_i} = \left(\frac{2}{T}\right)^{\frac{1}{2}} \left(\sum_{\ell=1}^{\frac{N}{2}} \frac{|\widetilde{B}_i^o(f_\ell)|^2}{S_n(f_\ell)}\right)^{\frac{1}{2}} \tag{31}$$

is the deflection ratio. Now, since $\frac{T}{N} = \Delta T = \frac{1}{F_s}$, we have:

$$d_i^2 = F_s\left(\frac{2}{N}\sum_{\ell=1}^{\frac{N}{2}} \frac{|\widetilde{B}_i^o(f_\ell)|^2}{S_n(f_\ell)}\right). \tag{32}$$

Since $\widetilde{B}_i^o(0) = 0$ due to the high-pass filter and noting that $\widetilde{B}_i(f_{\ell-1}) = \widetilde{B}_i^*(f_{N-\ell+1})$, the above expression can be rewritten equivalently as:

$$d_i^2 = F_s\left(\frac{1}{N}\sum_{\ell=1}^{N} \frac{|\widetilde{B}_i^o(f_\ell)|^2}{S_n(f_\ell)}\right). \tag{33}$$

If γ_1 and γ_2 are combined for the two planar directions, longitudinal and transverse, then $\gamma = \gamma_1 + \gamma_2$. But since γ_1 and γ_2 are statistically independent:

$$\begin{aligned} E(\gamma|H_0) &= 0; \quad E(\gamma|H_1) = m_1 + m_2; \\ \sigma^2(\gamma) &= \sigma^2(\gamma_1) + \sigma^2(\gamma_2). \end{aligned} \tag{34}$$

The corresponding deflection ratio is:

$$d^2 = F_s\left(\frac{1}{N}\sum_{\ell=1}^{N} \frac{|\widetilde{B}_1^o(f_\ell)|^2}{S_n(f_\ell)} + \frac{1}{N}\sum_{\ell=1}^{N} \frac{|\widetilde{B}_2^o(f_\ell)|^2}{S_n(f_\ell)}\right). \tag{35}$$

Therefore, $d = (d_1^2 + d_2^2)^{\frac{1}{2}}$, which represents the matched filter.